Int. J. Nonlinear Anal. Appl. In Press, 1–16
ISSN: 2008-6822 (electronic)
http://dx.doi.org/10.22075/ijnaa.2026.42241.5772

Evaluation of dust-removal performance for different particle-size diameters in industrial gravitational wet venturi scrubbers

Moein Roohbakhsh, Ali Reza Tahavvor*, Mohammad Mehdi Tavakol

Department of Mechanical Engineering, Shi.C., Islamic Azad University, Shiraz, Iran

(Communicated by Yasuo Narukawa)

Abstract

This study investigates the particle-removal performance of an industrial wet Venturi scrubber using CFD simulations. The main objective was to evaluate the effect of liquid injection through spray nozzles on flow hydrodynamics, pressure drop, and particle collection efficiency under identical operating conditions. The gas phase was modelled using the Realizable $k-\varepsilon$ turbulence model, while the nozzle-equipped configuration was simulated using the Volume of Fluid (VOF) model to resolve the transient gas-liquid flow. The Discrete Phase Model (DPM) was employed to track suspended pellet and direct reduced iron (DRI) particles with a polydisperse Rosin-Rammler size distribution in the range of $5-40\mu$m. Two configurations, with and without liquid-injection nozzles, were numerically compared. The results showed that the particle collection efficiency increased from 88.6% for the configuration without nozzles to 95.1% with liquid injection, while the pressure drop increased from 903.6 Pa to 1135.6 Pa. Despite the increase in pressure drop, the nozzle-equipped configuration achieved a higher particle collection efficiency and a lower fan-specific energy consumption per unit mass of removed particles. The findings demonstrate that liquid injection can substantially improve the particle-removal performance of the investigated Venturi scrubber, indicating its potential for suspended- particle removal applications in various industries.

Keywords: wet venturi scrubber, nozzle, dust removal, particle-size distribution, CFD, collection efficiency
2020 MSC: Primary 76T15; Secondary 76M12, 76T10

1 Introduction

No long-term solution can assess the social and environmental needs of communities located near industrial facilities, particularly in developing countries. Since the beginning of the Industrial Revolution, the global landscape of technology, innovation, and industry has undergone substantial changes that have markedly altered the traditional socioeconomic structure of society, especially in urban areas. Industrialization has had lasting positive and negative effects on society and the environment, including improved employment prospects and economic growth. However, it has also brought adverse effects such as greater pollution, greenhouse- gas emissions, health risks, and changes in local communities and lifestyles. Efficient tools and solutions must therefore be used to reduce the adverse effects

*Corresponding author
Email addresses: moein.roohbakhsh@iau.ir (Moein Roohbakhsh), ar.tahavvor@iau.ac.ir (Ali Reza Tahavvor), mm.tavakol@iau.ac.ir (Mohammad Mehdi Tavakol)

Received: August 2026 *Accepted:* September 2026

of industrial activities and advances. Accordingly, assessments of livability and environmental impacts have become essential tools for changing social and environmental domains. Given the complexity of industrial emissions from different sources, a new strategy is urgently required to reduce the effects of industrial gases on communities living near these areas [5].

One device used to reduce air pollution is the wet scrubber, which is widely applied in many industries because of its relatively high efficiency in removing fine particles (below 1μm), its ability to cool exhaust gases, and its suitability for corrosive or flammable industrial environments. As shown in Figure 1, a wet scrubber uses a liquid phase—usually water or a specific chemical solution—to absorb or wash solid particles and gaseous pollutants from the passing gas stream. The design and performance of these systems depend on several factors, including gas and liquid flow rates, nozzle type, ambient temperature, solution pH, and pollutant characteristics. Despite the widespread use of wet scrubbers, several challenges remain, including high energy and water consumption, corrosion, the need for wastewater treatment, and ineffective removal of some fine pollutants.

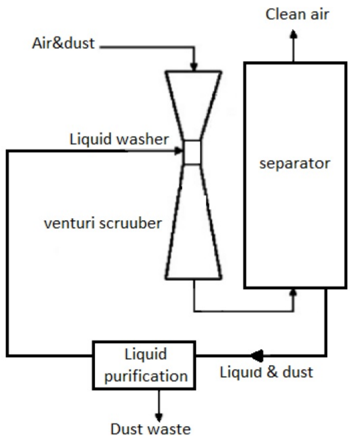

Figure 1: Gravitational wet Venturi scrubber

These issues have made more in-depth research necessary to optimize the performance and design of these systems and have led researchers toward advanced numerical modeling, such as computational fluid dynamics, and experimental testing under real operating conditions, because these approaches allow the pollutant-removal process to be better understood and controlled.

One of the main problems in wet scrubbers is the limited contact region among the solid, liquid, and gas phases. This limitation reduces particle-capture efficiency. More effective nozzle design, a larger contact area, and greater flow turbulence can therefore improve the performance of this process. Dynamic parameters such as pressure drop, gas velocity, and liquid-droplet diameter also have an important effect on the efficiency of this type of equipment.

A common configuration in wet scrubbers uses the Venturi region shown in Figure 2 to increase contact between the liquid and gas phases. In this design, the contaminated gas enters the Venturi throat at high velocity and collides with fine liquid droplets, thereby increasing absorption efficiency. The geometric dimensions of the Venturi, including the length and inlet diameter of the throat and the diverging section, directly affect the system performance parameters [18].

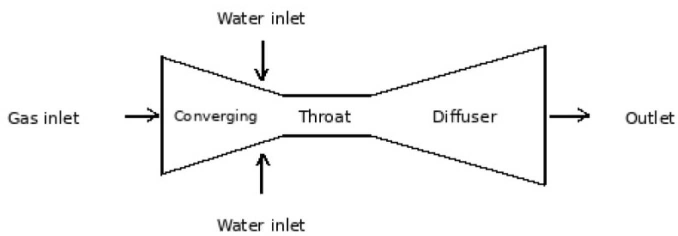

Figure 2: Schematic representation of a Venturi

These parameters determine not only pollutant-removal efficiency but also energy and water consumption. More specifically, although reducing the Venturi throat diameter increases gas velocity and improves turbulence and the contact area, it also produces a greater pressure drop that directly affects system power consumption. A larger pressure drop requires more powerful fans to convey the gas stream through the system, resulting in a substantial increase in electrical energy consumption. Determining the optimum relationship between removal efficiency and power consumption is therefore one of the main challenges in the design and operation of Venturi scrubbers. Excessive reduction of the throat diameter may also increase the required injection of scrubbing liquid to maintain stable operation, thereby increasing water consumption and wastewater generation. By contrast, Venturis with larger dimensions have a lower pressure drop and consume less energy, although their removal efficiency may also decrease under some conditions because the relative velocity and the collision rate between droplets and particles are reduced. Previous studies have focused mainly on particle-removal efficiency and have given less attention to the precise relationship between geometric parameters and energy–water consumption, although resource consumption, including water and energy, is critically important in industrial design. A major doctoral-level research problem is therefore the comprehensive quantitative investigation of how different factors affect operating parameters such as water consumption, fan power, and particle-removal efficiency. Such an analysis requires precise experiments and numerical simulations of multiphase gas–liquid–solid flows so that the interactions among scrubber geometry, flow hydrodynamics, gas–liquid interactions, and particle collection can be properly evaluated. In addition, developing empirical or semi-empirical models to predict system behavior on the basis of geometric dimensions can be highly useful for design and operation of Venturi scrubbers, particularly at industrial scale. Special models compatible with the environmental and economic conditions of each country should be developed for local climates and industries, especially in countries with limited water and energy resources, such as Iran.

A review of completed studies and the technical literature indicates that water consumption, power requirements, and Venturi dimensions are among the factors affecting scrubber efficiency.

2 Separator vessel

Inertial collectors operate on the principle that aerosol material in a carrier gas stream has greater inertia than the gas. Because the drag forces acting on a particle are a function of the particle diameter squared and the inertial forces are also a function of the diameter squared, it follows that the inertial force associated with removal becomes relatively greater as particle diameter increases. Inertial collectors are therefore most efficient for larger particles. Inertia is also a function of particle mass, and heavier particles are removed more efficiently by inertial collectors. The most common inertial collector is the cyclone, which is used in two basic forms: tangential entry and axial entry, as shown in Figure 3 (a and b) [3]. the radius of curvature and increasing the gas velocity both increase efficiency, these changes also increase the pressure drop across the collector. Designing inertial collectors for maximum efficiency at minimum cost and minimum pressure drop is a problem that lends itself to computer optimization.

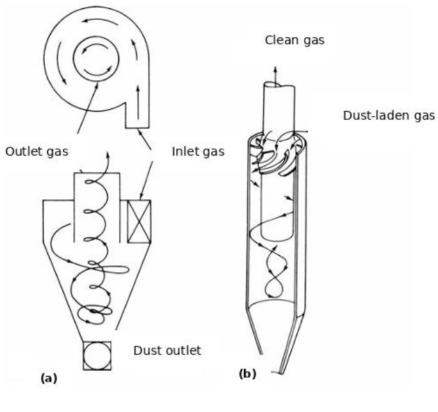

Figure 3: (a) Tangential-entry cyclone; (b) axial-entry cyclone

Fluid behavior is generally studied using two main approaches: experimental tests and numerical analyses. Much of the knowledge currently available in fluid mechanics is the result of years of observation, experimentation, and empirical investigation by researchers. The field has in fact developed and evolved gradually on the basis of the results of numerous tests and repeated experiments. In recent years, computational fluid dynamics (CFD) has been increasingly used alongside experimental methods as an effective tool for examining fluid-flow behavior, heat transfer, and other related phenomena. By means of numerical simulation, this approach allows flow conditions to be examined in greater detail and with greater precision, particularly when full-scale experiments are difficult or costly. CFD is now applied to many engineering and industrial problems. Vehicle and aircraft design, heat-exchanger performance, hydrodynamic systems, multiphase flows, power-plant equipment, and combustion processes can all be analyzed using this method. In general, any system involving fluid flow or heat transfer can be investigated and optimized using this approach [7, 9].

The main objective of this research is to develop an accurate and operational model of wet-scrubber performance in removing suspended particles by means of numerical approaches. In this model, the numerical effects of nozzle presence on dust-particle collection efficiency, energy consumption, and particle collection efficiency are analyzed and examined. The model should be capable of predicting performance under different operating conditions and should also provide recommendations for improving the design, reducing energy consumption, and increasing efficiency. This research can help industries such as the food industry and heavy industries such as steelmaking to reduce emissions and improve productivity, while also adding new scientific data to global knowledge. In view of the growing importance of air-pollution control and the need to develop relevant technologies, this research can contribute to the design of a new generation of wet scrubbers that are both efficient and sustainable.

3 Review of previous studies

Goel et al. developed an Eulerian-Lagrangian CFD model to simulate hydrodynamic behavior and mass transfer in a self-priming Venturi scrubber. The results showed that pressure drop and liquid loading were functions of the Reynolds number and that the model accurately predicted two-phase behavior and pressure variations in the converging and nozzle regions. Despite the reduction in liquid loading, increasing the air velocity improved particle-absorption efficiency because the number of droplets increased [10]. Tomaszewski et al. used CFD analysis to investigate the effect of spray-scrubber geometry on dust removal. They showed that the scrubber with one dust eliminator performed best; adding more eliminators altered the gas flow because of the increased local velocity but produced only a slight improvement in efficiency. The numerical results differed from the available data by less than 10% [18]. Attaullah et al. modeled a Venturi scrubber and showed that throat velocity, the liquid-to-gas ratio, and liquid entry had the greatest effects on pressure drop. Comparison with experimental data showed that the Mohibi model was more accurate than the Calvert model in predicting collection efficiency [3]. In an experimental study of absorption from biogas, Gantina et al. reported that the efficiency (99.5%) was obtained at a pressure of 4 bar and a water flow rate of 0.15 L/s, and that higher pressure and flow rate increased absorption efficiency [9]. Danzomo et al. performed a CFD simulation of a wet scrubber for the cement industry and showed that the velocity and pressure distributions in the system followed the principles of turbulent flow and that CFD simulation was a reliable approach for designing countercurrent wet scrubbers [7]. Hu and Gao investigated the performance of wet scrubbers with different numbers of blades and showed that the 16-blade scrubber provided the best combination of removal efficiency and minimum pressure drop. Field tests also confirmed a reduction in dust concentration [12]. Mukherjee and Verma showed for a submerged Venturi scrubber that increasing the liquid level, inlet dust concentration, and throat gas velocity increased removal efficiency. ANOVA also confirmed the model's predictive capability relative to the experimental data [15]. Rasanen et al. demonstrated that adding an auxiliary Venturi and improving droplet separation increased removal efficiency and reduced outlet dust, while higher nozzle- water pressure produced smaller droplets and increased particle collisions [16]. Khadra et al. used two-dimensional mass-transfer simulation and reported that increasing the gas velocity and reducing the liquid flow rate increased pollutant-removal efficiency from biomass gas [13]. Ahad et al. investigated the effect of Venturi geometry on iodine-particle removal and showed that the orifice diameter was the most influential parameter affecting the mass- transfer rate, followed by the orifice-plate position and the length of the converging section [1]. In a review study, Avinasilingam and Gopalsamy concluded that converging-section design, Venturi height, and selection of an appropriate turbulence model were the principal factors affecting efficiency and pressure drop [4]. Wansom et al. showed in a smart hybrid scrubber that increasing the air-to-liquid ratio and turbulence and reducing droplet size improved absorption efficiency, whereas packing materials had little effect because they enlarged the droplets [20]. Mestemaker and Elmazi modeled a wet scrubber for engine exhaust gas and showed that the system could maintain stable removal, although evaporation in the packed bed could cause momentary performance instability [14]. Hoyos et al. designed a small- scale scrubber and showed that the submicron-particle collection trend remained similar to that of an industrial scrubber, although the absolute efficiency was lower [11]. Cao and Wang proposed a new pressure-drop model for a fog-annular Venturi. The results showed that boundary-layer separation and Kelvin-Helmholtz instability could increase energy losses and that the modified model had an error below 17% [6]. Darbandi et al. showed that increasing salt concentration, lowering solution temperature, and increasing packed-bed height improved fine-particle removal efficiency [8]. Telin and Lin used CFD modeling of a centrifugal scrubber and showed that increasing the contact opening and adding moisture could increase heat recovery by up to 9%, while the new compact design could reduce dimensions and increase thermal efficiency [17].

4 Research method

In this study, suspended pellet and sponge-iron particles in the exhaust gases generated by the operating processes of a steel plant were investigated for different particle- size classifications. To achieve the research objectives, a simple Venturi scrubber was numerically simulated and analyzed in nozzle-equipped and nozzle-free configurations. The flow behavior and the mechanisms involved in pollutant contact, mixing, and capture were examined by numerical simulation. The overall research framework was developed on the basis of an analysis of the operating parameters affecting scrubber performance, similar to those reported in previous studies of Venturi scrubbers, wet scrubbers, and heat-recovery systems [1, 3, 4, 5, 6, 7, 8, 9, 10, 11, 12, 13, 14, 15, 16, 17, 18, 20].

4.1 Geometry and configuration of the venturi scrubber

The Venturi-scrubber geometry for the nozzle-equipped and nozzle-free configurations was created in SolidWorks, as shown in Figure 4 (a and b), and was then meshed for CFD analysis. A three-dimensional wet venturi scrubber was investigated to evaluate its hydrodynamic behavior, pressure drop, and particle collection efficiency for the removal of pellet and direct reduced iron (DRI) particles generated from an industrial steel production process. The investigated venturi scrubber geometry consists of five main sections: the inlet section, converging section, throat section, diverging section, and separator section. After entering the inlet section with an inlet diameter of 0.7 m, the gas flow passes through the converging section with a length of 1.5 m. Due to the reduction in cross- sectional area, the gas velocity increases along this section. The converging section has convergence angles of 38° in the y-z plane and 29.44° in the x-y plane, resulting in a gradual contraction of the flow passage and acceleration of the gas stream. The accelerated gas flow then enters the throat section, where the maximum gas velocity is achieved. The throat section has a hydraulic diameter of 0.3042 m and a length of 0.712 m. In this region, the washing water is injected into the gas stream through six nozzles with a diameter of 0.0266 m. The high gas velocity in the throat promotes liquid atomization, droplet formation, and intensive gas-liquid interactions, leading to enhanced particle-droplet collisions and improved particle collection performance. After passing through the throat section, the two-phase flow enters the diverging section with a length of 3 m, where the gas velocity decreases and part of the static pressure is recovered. The diverging section has divergence angles of 5.06° in the y-z plane and 8° in the x-y plane, which significantly influence pressure recovery and the development of the downstream flow field. Finally, the gas-liquid-particle mixture enters the separator section with a diameter of 2.1 m and a length of 5 m, where the separation of particles and liquid droplets from the gas phase is completed. The main geometric dimensions of the Venturi scrubber and separator are summarized in Table 1.

Table 1: Geometric dimensions of the Venturi scrubber and separator

Region / Parameter	Dimension	Unit
Inlet diameter	0.7	m
Outlet diameter	0.71	m
Separator diameter	2.1	m
Separator length	5	m
Overall Venturi assembly length	7.084	m
Converging-section length	1.5	m
Diverging-section length	3	m
Throat hydraulic diameter	0.3042	m
Throat length	0.712	m
Convergence angle in the y-z plane	38	°
Convergence angle in the x-y plane	29.44	°
Divergence angle in the y-z plane	5.06	°
Divergence angle in the x-y plane	8	°
Number of nozzles	6	–
Nozzle diameter	0.0266	m
Throat-to-inlet hydraulic diameter ratio $\beta = D_t/D_{in}$	0.4346	–
Throat length-to-hydraulic-diameter ratio l_t/D_{in}	2.34	–
Outlet-to-throat hydraulic diameter ratio D_{out}/D_t	2.33	–

4.2 Mesh generation

To ensure the reliability of the numerical results and minimize the influence of mesh resolution on the solution, a grid independence study figure (4 a and b) was performed for geometrical configurations. A polyhedral mesh was used. The mesh-independence test was performed as shown in Figure 5 and Figure 6. Therefore, the mesh with a minimum and maximum cell size of 0.007 m and 0.16 m, and 190333 nodes respectively, was selected as the optimum computational grid for the subsequent simulations. The main characteristics and quality parameters of the final meshes used are summarized in Tables 2.

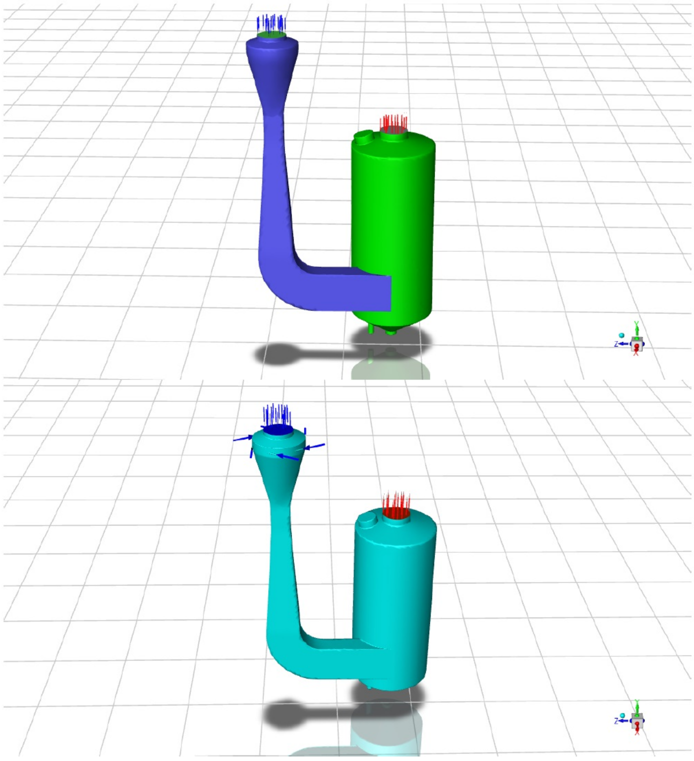

Figure 4: (a and b) Simple Venturi scrubber without and with nozzles

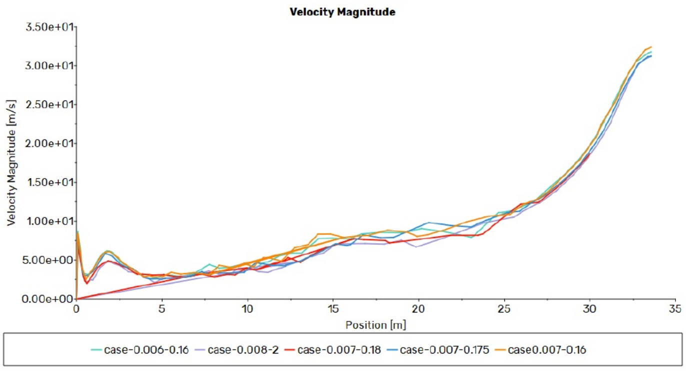

Figure 5: Mesh-independence test chart for the Venturi-scrubber mesh solution

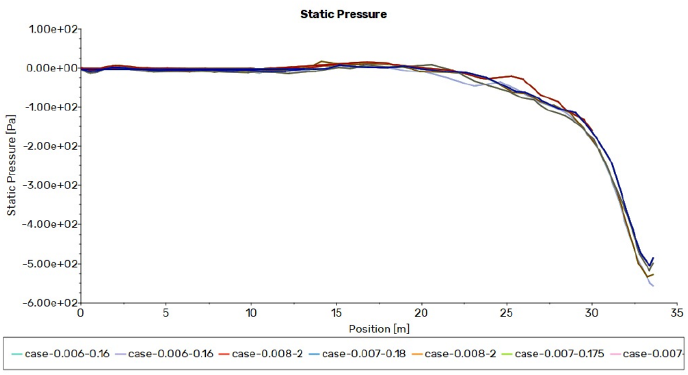

Figure 6: Mesh-independence test chart for the Venturi-scrubber mesh solution

Table 2: Venturi-scrubber mesh quality

	Number of computational nodes	Mesh orthogonality	Mesh skewness
1	181887	0.9406705	0.021510918
2	186403	0.9473028	0.021590557
3	184853	0.94732333	0.02184943
4	190333	0.94695625	0.021092736
5	190290	0.94696272	0.020913929

4.3 Physical model and governing equations

4.3.1 Multiphase formulation

the multiphase formulation used in this study consisted of an Eulerian description of the continuous gas-liquid phase and a Lagrangian description of the suspended solid particles [10]. The gas and liquid phases were treated as continuous, immiscible phases and were solved using the Volume of Fluid (VOF) model for the nozzle-equipped configurations [13]. Thus, VOF was used to resolve the transient gas-liquid interface and the spatial distribution of the liquid phase during water injection. The suspended pellet and direct reduced iron (DRI) particles were treated as a discrete phase and tracked individually using the Discrete Phase Model (DPM) [19] within the Lagrangian framework. Therefore, the liquid droplets generated by water injection were not represented as individual DPM particles; rather, they originated from the resolved continuous liquid phase in the VOF calculation. The interaction between the discrete solid particles and the continuous phase was enabled in the DPM formulation. Accordingly, the continuous-phase solution provided the local velocity and flow-field information required for particle tracking, while the momentum exchange associated with the discrete particles was included in the continuous-phase momentum equation through the corresponding DPM source term. The particle trajectories were subsequently calculated based on the local continuous-phase velocity field and the forces acting on the particles, primarily drag and gravity.

4.3.2 Continuous-phase governing equations

The conservation equations of mass and momentum were used to describe the continuous-phase flow. The continuity equation (conservation of mass) is:

$$\partial\rho/\partial t + \nabla\cdot(\rho u) = S_m \tag{4.1}$$

in which, ρ is the density of the continuous phase, $\vec{u}$ is the velocity vector, t is time, and S_m is the mass source term. The present study did not consider interphase mass transfer, evaporation, or condensation. Therefore, the mass source term was set to zero $S_m = 0$. For the VOF simulations, the two phases of the gas and liquid were simulated as immiscible fluids and no interphase mass transfer was considered. The conservation of momentum for the continuous phase is expressed as:

$$\partial(\rho u)/\partial t + \nabla\cdot(\rho uu) = -\nabla p + \nabla\cdot\tau + \rho g + S_{DPM} \tag{4.2}$$

in which p is the static pressure, τ is the viscous stress tensor, S_{DPM} is the momentum exchange between the continuous phase and the discrete particles, and g is the gravitational acceleration.

4.4 Turbulence model

The turbulent flow was modeled using the Realizable $k-\varepsilon$ turbulence model [1]. This model was selected because of its suitability for complex turbulent flows involving strong pressure gradients, flow separation, and highly distorted flow fields, which are characteristic of Venturi scrubbers.

$$\frac{\partial(\rho k)}{\partial t} + \nabla\cdot(\rho k\vec{V}) = \nabla\cdot\left[\left(\mu + \frac{\mu_t}{\sigma_k}\right)\nabla k\right] + G_k - \rho \tag{4.3}$$

where G_k is the generation of turbulent kinetic energy and μ_t is the turbulent viscosity. The transport equation for the turbulent dissipation rate ε is:

$$\frac{\partial(\rho\varepsilon)}{\partial t} + \nabla\cdot(\rho\varepsilon\vec{u}) = \nabla\cdot\left[\left(\mu + \frac{\mu_t}{\sigma_\varepsilon}\right)\nabla\varepsilon\right] + \rho C_1 S\varepsilon - \rho C_2\frac{\varepsilon^2}{k+\sqrt{\nu\varepsilon}} \tag{4.4}$$

where σ_k and σ_ε are the turbulent Prandtl numbers C_1 and C_2 are model constants, S_ε is a strain-rate-related term, and ν is the kinematic viscosity. The turbulent viscosity, μ_t represents the additional momentum transport caused by turbulent velocity fluctuations and is used to account for the effect of turbulence on the mean flow field. In the

Realizable $k-\varepsilon$ model, the turbulent viscosity is calculated from the local turbulent kinetic energy and its dissipation rate as:

$$\mu_t = \rho C_\mu k^2/\varepsilon \tag{4.5}$$

μ_t is evaluated as a function of the local flow conditions rather than being assigned a fixed constant.

4.5 Volume of fluid (VOF) model

The nozzle-equipped Venturi scrubber configuration was numerically simulated using the Volume of Fluid (VOF) model to resolve the transient gas-liquid flow and the evolution of the water-gas interface during liquid injection. The gas and liquid phases were treated as continuous, immiscible phases, with air defined as the primary phase and water as the secondary phase. The VOF model solves a volume-fraction transport equation in each computational cell to determine the spatial distribution of the phases. For incompressible flow without interphase mass transfer, the volume-fraction equation for the liquid phase is given by:

$$\frac{\partial \alpha_l}{\partial t} + \nabla \cdot (\alpha_{lu}) = 0 \tag{4.6}$$

here α_l is the liquid volume fraction and $\mathbf{u}$ is the local mixture velocity. volume fraction is obtained from the volume-fraction constraint:

$$\alpha_g + \alpha_l = 1 \tag{4.7}$$

Water was injected through six identical TF-series nozzles at a prescribed velocity of 2.5m/s, with the injection direction normal to the gas-flow direction at the nozzle outlet. The main geometrical and operating specifications of the nozzles are provided in Table 3. The configuration and geometry of the TF-series nozzle used in the simulations are shown in Fig. 7. The liquid phase was resolved using the VOF formulation. Since the liquid phase was resolved directly by the VOF model, no initial droplet-size distribution or Sauter mean diameter was prescribed, and no empirical or semi-empirical droplet-breakup model was employed. Instead, the liquid structures and droplet characteristics developed directly from the calculated gas-liquid flow field. The resulting droplet diameters in the separator region were approximately $58.6-60\mu m$, and their distribution is presented in Fig. 8.

Figure 7: Configuration and geometry of the TF-series nozzle used for liquid injection.

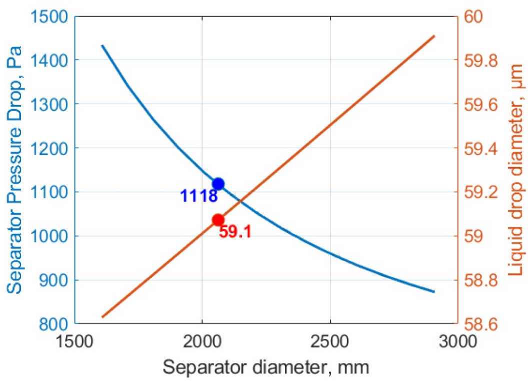

Figure 8: Droplet diameter distribution obtained in the separator region from the VOF simulation

4.6 Discrete phase model and particle motion

The trajectory of each particle was obtained by integrating its equation of motion through the continuous-phase flow field. Since Drag and Gravity were included as the particle forces the particle equation of motion can be written as

$$m_p \frac{du_p}{dt} = F_D + F_G \tag{4.8}$$

F_D and F_G are the drag and gravitational forces, respectively, acting on the particle. Relative velocity between the particles and the surrounding continuous phase was used to determine the particle trajectories. This formulation allows the particle transport and collection characteristics to be studied in the flow conditions inside the Venturi scrubber.

The drag force acting on a spherical particle is expressed as:

$$F_D = \frac{1}{2} C_D \rho A_p |u - u_p|(u - u_p) \tag{4.9}$$

$$C_D = \frac{24}{Re_p}(1 + 0.15 Re_p^{0.687}), \qquad Re_p < 1000 \tag{4.10}$$

$$C_D = 0.44, \qquad Re_p \geq 1000 \tag{4.11}$$

where C_D is the drag coefficient, A_p is the projected area of the particle, ρ is the continuous- phase density, and $u - u_p$ represents the relative velocity between the continuous phase and the particle. The particle Reynolds number was calculated as:

$$Re_p = \frac{\rho d_p \, |u - u_p|}{\mu} \tag{4.12}$$

where d_p is the particle diameter and μ is the dynamic viscosity of the continuous phase.

The momentum exchanged between the discrete particles and the continuous phase is incorporated into the continuous-phase momentum equation through the DPM source term:

$$S_{DPM} = -\frac{1}{V_c} \sum_p \Delta P \tag{4.13}$$

where V_c is the volume of the computational cell, and ΔP represents the change in particle momentum resulting from its interaction with the continuous phase.

A total of 61,000 computational particles were injected from the gas-inlet boundary in each simulation. These particles represent computational DPM parcels used to sample the suspended-particle population and do not correspond to the exact physical number of particles in the exhaust stream. The same number of computational particles was used for both configurations to provide a consistent basis for comparison. A two-way coupling approach was adopted between the discrete solid particles and the continuous phase. Accordingly, the momentum exchange associated with the discrete particles was incorporated into the continuous-phase momentum equation through the DPM source terms, allowing the effect of particle transport on the continuous-phase flow field to be accounted for during the numerical solution. Particle collection was evaluated based on the final fate of the tracked discrete particles at the computational boundaries. Particles classified as Trapped were considered collected, whereas particles classified as Escaped through the outlet boundary were considered uncollected. Accordingly, the particle collection efficiency was calculated as:

$$\eta_N = \frac{N_{trap}}{N_{trap} + N_{escape}} \times 100 \tag{4.14}$$

represent the numbers of computational particles classified as trapped and escaped, respectively. The collection efficiency was determined directly from the particle fate obtained from the DPM calculation. No separate deterministic or stochastic particle- droplet collision or capture model was employed. Therefore, particle collection was evaluated from the computed Lagrangian particle trajectories and their final boundary status (Trapped or Escaped).

4.7 Dimensionless parameters

To characterize the flow regime and particle- transport behavior in the Venturi scrubber, the relevant dimensionless parameters were considered. The gas Reynolds number was used to characterize the flow regime and was calculated as:

$$Re_g = \frac{\rho_g U D_h}{\mu_g} \tag{4.15}$$

where ρ_g, U, D_h, and μ_g are the gas density, characteristic gas velocity, hydraulic diameter, and dynamic viscosity, respectively. The Stokes number was used to characterize the ability of suspended particles to follow changes in the gas- flow field and was defined as:

$$St = \frac{\tau_p U}{L} \tag{4.16}$$

where τ_p is the particle response time, U is the characteristic gas velocity, and (L) is the characteristic length scale. For the particle Reynolds numbers considered in the present study, the particle response was evaluated consistently with the drag formulation used in the DPM model.

The relevant dimensionless parameters were used to provide a physical interpretation of the gas-flow regime and particle inertial response in the investigated Venturi-scrubber configurations.

4.8 Boundary conditions and operating parameters

the flow and boundary conditions were established to simulate the flow characteristics of the industrial-scale wet Venturi scrubber investigated in this study. A consistent set of operating conditions was applied for all simulated cases to enable a reliable comparison of the effects of liquid injection on hydrodynamic behavior, pressure drop, and particle collection efficiency Based on previous studies [17]. A velocity-inlet boundary condition was applied at the gas inlet, with an inlet velocity of 17.3 m/s and a inlet turbulence intensity of 2.3%. The specified turbulence intensity represents the relative magnitude of velocity fluctuations at the inlet and is independent of the selected Realizable $(k-\varepsilon)$ turbulence model, while a pressure outlet boundary condition was imposed at the gas outlet. For the nozzle-equipped configuration, water was injected through six velocity-inlet boundaries at a prescribed velocity of 2.5 m/s.

The operating conditions and thermophysical properties of the gas phase, liquid phase, and suspended solid particles used in the numerical simulations are summarized in Table 3. These parameters include operating pressure, temperature, gas inlet velocity, liquid injection conditions, particle density, particle mass flow rate, and particle- size distribution parameters.

Table 3: Input parameters and boundary conditions used in the numerical simulation

Parameter	**Value**
Ambient temperature	$45°C$
Pressure	82603 Pa
Gas inlet velocity	17.3 m/s
Inlet turbulence intensity	2.3%
Air density	$0.904 kg/m^3$
Air dynamic viscosity	$1.9 \times 10^{-5} Pa \cdot s$
Suspended-particle density	$2500 kg/m^3$
Suspended-particle mass flow rate	0.1865 kg/s
Number of nozzles	6
Water inlet velocity at each nozzle	2.5 m/s
spray angle	90°
internal diameter of each nozzle	0.0266 m
Water–air interfacial surface tension	0.073 N/m

The suspended pellet and direct reduced iron (DRI) particles were modeled using the Discrete Phase Model (DPM). The particles were injected from the gas inlet boundary, and their trajectories were calculated by integrating the particle equation of motion within the continuous- phase flow field. Drag and gravitational forces were considered as the dominant forces governing particle motion, while the momentum exchange between the discrete particles and the continuous phase was incorporated through the DPM source terms.

The particle- size distribution was defined using the Rosin-Rammler distribution [2, 19] to represent the polydisperse nature of the suspended particles in the industrial exhaust stream. The cumulative distribution was defined as:

$$F(d_\mathrm{p}) = 1 - \exp\left[-\left(\frac{d_\mathrm{p}}{d_\mathrm{c}}\right)^{\mathrm{n}}\right] \tag{4.17}$$

where $\mathrm{F(d_p)}$ is the cumulative particle fraction below diameter $\mathrm{d_p}$, $\mathrm{d_p}$ is the particle diameter, d_c is the characteristic diameter, and n is the dimensionless spread parameter. In the present simulations, $d_c = 10\mu m$ and $\mathrm{n} = 3.5$ were used, with the particle diameter limited to $5 - 40\mu m$.

The characteristic diameter and spread parameter were specified in the numerical model.

Table 4: Particle size distribution based on Rosin-Rammler model for the $5-40\mu m$ particle-size range

Particle size range (μm)	**Particle fraction %**
5-10	42.3
10-20	49.4
20-30	7.9
30-40	0.4
total	100

The Venturi-scrubber performance was evaluated using particle collection efficiency, pressure drop, water consumption, and fan-specific energy consumption. Collection efficiency was determined from the final DPM particle fate, with Trapped particles considered collected and Escaped particles considered uncollected. Pressure drop was calculated from the difference between the mean static pressures at the inlet and outlet. Water consumption was represented by the specified liquid mass flow rate, while fan-specific energy consumption was estimated using the installed 24-kW fan power and the mass flow rate of removed particles.

4.9 Numerical solution method

The numerical simulations were performed using ANSYS Fluent 2024 R1. to investigate the effect of liquid injection through the nozzles on flow hydrodynamics, pressure drop, and particle collection efficiency, numerical simulations were performed for two different Venturi scrubber configurations: (i) without liquid-injection nozzles and (ii) with liquid-injection nozzles. In both configurations, the main geometry and operating conditions were kept constant, and gravitational effects were considered. The presence or absence of liquid injection was the only major modeling difference between the two configurations, allowing its effect on scrubber performance to be evaluated under comparable operating conditions. Due to the absence of liquid injection, the configuration without nozzles was simulated under steady-state conditions, with the gas phase and suspended solid particles considered in the computational domain. For the nozzle-equipped configuration, The Volume of Fluid (VOF) model was employed to simulate water injection and the resulting gas-liquid flow. Air was treated as the primary phase and water as the secondary phase. The DPM model was used in both configurations to track the suspended solid particles within the continuous-phase flow field. The main solver settings, numerical schemes, and operating parameters used for the two configurations are summarized in Table 5.

Table 5: Summary of the numerical solver settings applied to the two groups of simulations

Parameter	**Without nozzle configuration**	**Nozzle-equipped configuration**
Solver type	Pressure-based	Pressure-based
Solution method	Steady-state	Transient
Pressure–velocity coupling scheme	Coupled	PISO
Multiphase approach	Single-phase + DPM	VOF + DPM
Pressure discretization scheme	Second-order	PRESTO!
Momentum discretization scheme	Second-order Upwind	Second-order Upwind
Turbulence equations discretization scheme	First-order Upwind	First-order Upwind
Velocity formulation	Absolute	Absolute
Gravity	Enabled	Enabled
Surface tension coefficient	–	0.073 N/m
Nozzle boundary condition	–	Velocity inlet
Water injection velocity	–	2.5 m/s
Particle tracking model	DPM (Lagrangian)	DPM (Lagrangian)
Particle size distribution	Rosin–Rammler	Rosin–Rammler

The convergence of the numerical solutions was assessed based on the residuals of the governing equations and the stabilization of the main monitored quantities, including pressure drop and particle collection efficiency. The numerical convergence criteria and solution settings were defined according to the flow configuration. For the nozzle-free configuration, the simulations were performed under steady-state conditions with a maximum of 1000 iterations and a reporting interval of 1. For the nozzle-equipped configuration, the simulations were performed using a time-step size of $\Delta t = 0.001$, $t = 0.001s$, with 100-time steps, corresponding to a total physical simulation time of 0.1s, and a maximum of 30 iterations per time step. In both configurations, the normalized residual convergence criterion was set to 10^{-3}. The pressure drop was monitored throughout the simulations to assess the convergence and stabilization of the numerical solution. These numerical settings were applied consistently to the corresponding simulations.

Residual Convergence Criterion:

$$R_\Phi = \frac{|R_\Phi|}{|R_{\Phi,0}|} < 10^{-3} \tag{4.18}$$

Total Simulation Time for the Nozzle-Equipped Configuration:

$$t_{\text{total}} = N_t \Delta t \tag{4.19}$$

Relative Pressure-Drop Variation for Assessing Solution Stabilization:

$$\varepsilon_{\Delta p} = \frac{|\Delta p^n - \Delta p^{n-1}|}{|\Delta p^{n-1}|} \times 100 \tag{4.20}$$

4.10 Data analysis

Finally, the effect of nozzle presence on removal efficiency and pressure drop was examined independently. Statistical analysis and sensitivity plots were used for this purpose. The ultimate objective was to identify the optimum combination for achieving the removal efficiency.

5 Results and discussion

5.1 Flow pattern and particle behavior in different configurations

5.1.1 Venturi scrubber without nozzles

Figure 9 shows the flow path and velocity distribution in the Venturi scrubber without nozzles. In this configuration, the flow enters the throat after passing through the converging section and undergoes an increase in velocity. However, because no nozzles are present and no mechanisms enhance mixing in the outlet region, effective contact between the pollutant particles and liquid droplets remains limited. Consequently, some particles pass through the system without sufficient collision.

The particle-trajectory results showed that, of the 61000 particles injected, 54046 were collected in the system and 6954 escaped through the outlet. The collection efficiency in this configuration was therefore 88.6%. The maximum particle velocity at the throat was also reported to be approximately $63m/s$. These results indicate that, in the absence of nozzles, the intensity of interphase interaction is insufficient for effective particle removal despite local acceleration in the throat region.

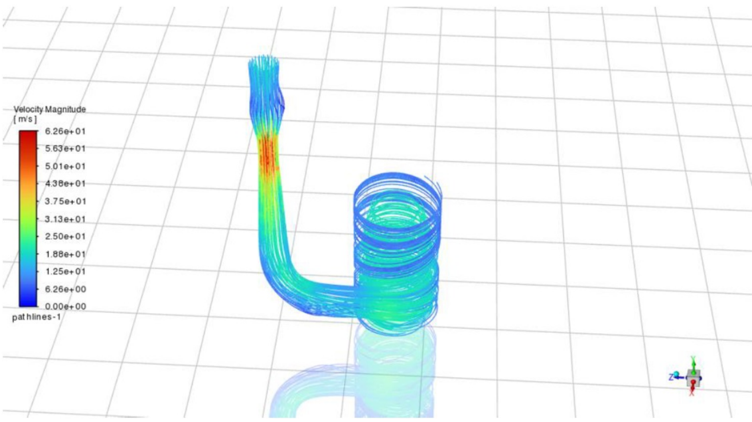

Figure 9: Streamlines and velocity variations in the simple Venturi scrubber without nozzles

5.1.2 Nozzle-equipped venturi scrubber

Figure 10 presents the flow distribution for the simple nozzle-equipped Venturi scrubber. Adding the nozzles increased flow concentration, intensified acceleration in the throat region, and strengthened local turbulence. These changes increased the probability of collision between pollutant particles and liquid droplets and thereby improved collection efficiency.

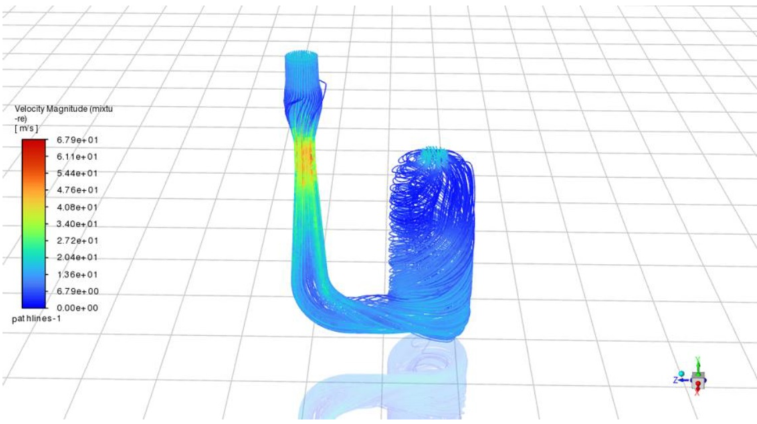

Figure 10: Streamlines and velocity variations in the simple Venturi scrubber with nozzles

According to the simulation results, the maximum particle velocity in this configuration reached 67.9 m/s, and the number of particles escaping from the system decreased to 2989. Collection efficiency consequently increased to 95.1%. By creating a more intense flow field and increasing the mixing rate, the nozzles therefore improved particle-removal performance.

5.2 Pressure drop and its effect on scrubber performance

The pressure drop across the Venturi scrubber was calculated from the difference between the area-averaged static pressures at the inlet and outlet sampling planes. The pressure drop was defined as:

$$\Delta p = \overline{p_{in}} - \overline{p_{out}} \tag{5.1}$$

where p_{in} and p_{out} are the area-averaged static pressures at the inlet and outlet sampling planes, respectively. The area-averaged static pressure was calculated as:

$$\overline{p} = \frac{\int_A p dA}{\int_A dA} \tag{5.2}$$

where p is the local static pressure and A is the cross-sectional area of the corresponding sampling plane. Static pressure was used rather than total pressure for evaluating the pressure drop. The same inlet and outlet sampling planes were used for all simulated configurations to ensure a consistent comparison. Pressure drop is a key performance indicator for Venturi scrubbers because it is associated with the aerodynamic energy required to accelerate the gas and promote gas-liquid interaction, and consequently with the power requirement of the fan or blower. An increase in pressure drop generally indicates greater momentum transfer and stronger flow acceleration through the throat, which can promote liquid dispersion, gas-liquid mixing, and particle- droplet interactions. However, excessive pressure drop is undesirable because it increases the required operating power and associated energy losses. Therefore, Venturi-scrubber design requires a balance between particle collection According to the results presented in Fig. 11 (a,b) and Table 6, the comparison of the two configurations shows that the baseline configuration without liquid injection exhibited a lower particle collection efficiency and a greater number of particles escaping from the system. The introduction of water through the nozzles increased the gas-liquid interaction and improved the conditions for particle-droplet collisions, resulting in an increase in collection efficiency to 95.1%. efficiency and pressure drop. The calculated pressure drop was 903.59 Pa for the Venturi scrubber without nozzles and 1135.60 Pa for the nozzle- equipped configuration. Thus, the introduction of liquid increased the pressure drop by approximately 25.7%. This increase is attributed to the additional resistance and momentum exchange associated with the injected liquid phase and the resulting gas-liquid interaction. Despite the increase in pressure loss, the nozzle-equipped configuration provided a substantial improvement in particle collection efficiency, indicating a favorable trade-off between collection performance and pressure loss under the investigated operating conditions.

From the standpoint of the operating mechanism, the presence of liquid injection nozzles enhanced particle removal by promoting liquid dispersion and gas-liquid mixing, thereby increasing the probability of contact and collision between suspended particles and the liquid phase. The nozzle-equipped configuration therefore demonstrated improved particle-removal performance compared with the configuration without liquid injection, although this improvement was accompanied by a higher pressure drop.

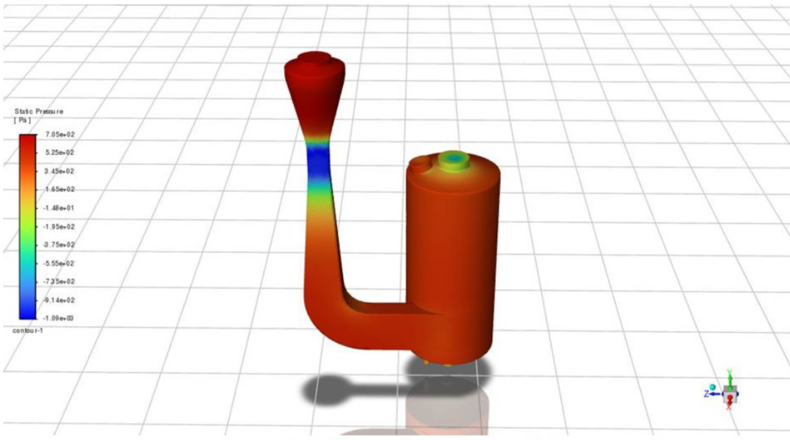

(a). Venturi scrubber without nozzles

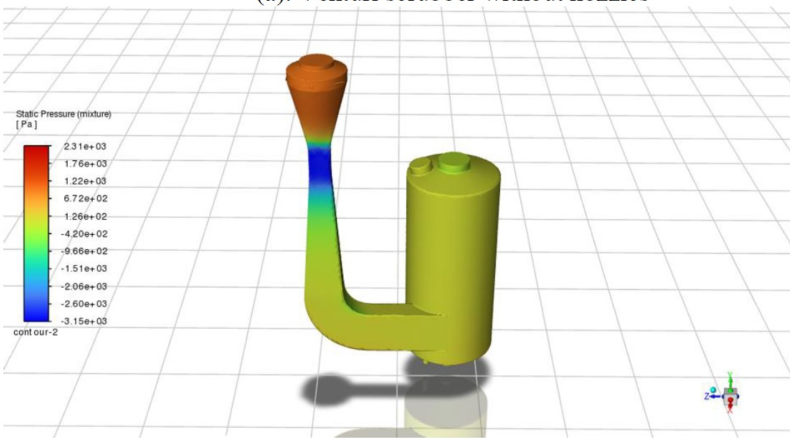

(b). Venturi scrubber with nozzles

Figure 11: (a). Venturi scrubber without nozzles, (b). Venturi scrubber with nozzles

Table 6: Different pressure-drop values for the Venturi scrubbers investigated

Venturi scrubber without nozzles	903
Venturi scrubber with nozzles	1135

5.3 Water consumption and liquid-to-gas ratio

For the nozzle-equipped configuration, water was introduced through six velocity-inlet nozzle boundaries at an inlet velocity of 2.5 m/s. The internal diameter of each nozzle was 0.0266 m. Accordingly, the volumetric flow rate through each nozzle was calculated from the nozzle cross-sectional area and the prescribed inlet velocity as:

$$Q_{L,n} = A_n V_n \tag{5.3}$$

where A_n is the cross-sectional area of the nozzle and V_n is the water inlet velocity. The corresponding mass flow rate was calculated as:

$$\dot{m}_{L,n} = \rho_L A_n V_n \tag{5.4}$$

Using a water density of approximately $1000 kg/m^3$, the calculated mass flow rate was approximately $1.39 kg/s$ per nozzle. For six nozzles, the total liquid mass flow rate was therefore approximately $8.32 kg/s$. The gas mass flow rate was calculated from the gas inlet cross-sectional area, inlet velocity, and gas density. For an inlet diameter of 0.7 m, an inlet velocity of 17.3 m/s, and an air density of $0.904 kg/m^3$, the resulting gas mass flow rate was approximately $6.02 kg/s$. Therefore, the liquid-to-gas mass ratio was:

$$L/G = \frac{\dot{m}_L}{\dot{m}_g} = \frac{8.32}{6.02} \approx 1.38 \tag{5.5}$$

The specific water consumption was also evaluated based on the mass of particles removed from the gas stream. For a particle mass flow rate of $0.1865kg/s$ and a collection efficiency of 95.1%, the removed particle mass flow rate was:

$$\dot{m}_{dust,removed} = \eta \dot{m}_p = 0.951 \times 0.1865 = 0.1774\text{kg/s} \tag{5.6}$$

Accordingly, the specific water consumption was approximately:

$$W_{spec} = \frac{\dot{m}_L}{\dot{m}_{dust,removed}} \approx 46.9\text{kg water/kg removed dust} \tag{5.7}$$

these quantities provide a quantitative basis for evaluating the water requirement and liquid-to-gas ratio of the nozzle-equipped Venturi scrubber.

5.4 Fan power and specific fan energy consumption

The installed fan power of the investigated Venturi-scrubber system was 24 kW and was considered identical for both configurations. Since the actual electrical power consumption of the fan was not measured separately for each operating condition, the installed fan power was used as the basis for estimating the fan specific energy requirement. The energy analysis in the present study was limited to the fan power associated with gas handling.

$$SEC_{fan} = \frac{P_{fan}}{\dot{m}_{dust,removed} \times 3600} \tag{5.8}$$

The calculated fan power, removed dust mass flow rate, and fan-specific energy consumption for the two investigated configurations are summarized in Table 7.

Table 7: Comparison of fan power, removed dust mass flow rate, and fan- specific energy consumption between the investigated configurations

Parameter	**Without nozzles**	**With nozzles**
Fan power	24 kW	24 kW
Removed dust mass flow rate	0.1652 kg/s	0.1774 kg/s
Fan-specific energy consumption	0.0404 kWh/kg	0.0376 kWh/kg

For the configuration without nozzles, the removed particle mass flow rate was 0.1652 kg/s, resulting in a fan-specific energy consumption of 0.0404 kWh/kg removed dust. For the nozzle-equipped configuration, the removed particle mass flow rate increased to 0.1774 kg/s, corresponding to a fan-specific energy consumption of 0.0376 kWh/kg removed dust. Thus, although the fan power was identical for both configurations, the higher particle collection efficiency of the nozzle-equipped configuration resulted in a lower fan-specific energy consumption per unit mass of removed dust.

The reported values represent a fan-power-based performance metric and should not be interpreted as the total energy consumption of the complete wet-scrubber system. Pumping power associated with liquid injection was outside the scope of the present energy analysis.

6 Conclusion

The results showed that the addition of liquid-injection nozzles improved the particle collection performance of the Venturi scrubber. The collection efficiency increased from 88.6% for the nozzle-free configuration to 95.1% for the nozzle-equipped configuration, while the pressure drop increased from 903 Pa to 1135 Pa. These results indicate that liquid injection can enhance particle removal under the investigated operating conditions, although this improvement is accompanied by an increase in pressure drop. Therefore, the nozzle-equipped configuration can be considered a suitable option for applications requiring improved particle collection efficiency under comparable operating conditions.

References

[1] J. Ahad, A. Farooq, W. Siddique, A. Ahmed, M. Ahmad, K. Waheed, K.R. Qureshi, and N. Irfan, *Influence of variation in converging section and orifice plane on the performance of venturi scrubber by using CFD*, Prog. Nuclear Energy **151** (2022), 104323.

[2] M. Alderliesten, *Mean particle diameters. Part VII. The Rosin-Rammler size distribution: physical and mathematical properties and relation-ships to moment-ratio defined mean particle diameters*, Particle Particle Syst. Character. **30** (2013), no. 3, 244–257.

[3] N.A. Attaullah, M.B.K. Niazi, M. Ahsan, and M. Ali, *Computational fluid dynamics simulation for the prediction of the venturi scrubber performance using finite volume method*, Int. J. Comput. Sci. Math. **11** (2020), no. 4, 338–346.

[4] M. Avinasilingam and S. Gopalsamy, *Studies on venturi scrubber performance and efficiency-a review*, J. Adv. Mech. Sci. **1** (2022), no. 1, 14–20.

[5] M. Bal and B.C. Meikap, *Prediction of hydrodynamic characteristics of a venturi scrubber by using CFD simulation*, South Afr. J. Chem. Eng. **24** (2017), no. 1, 222–231.

[6] R. Cao, H. Wang, R. Gong, Z. Jiang, H. Zhang, J. Zhu, and Y. Song, *Pressure drops model of gas-liquid phase for Venturi scrubber in fog-annular flow*, Chem. Eng. Res. Design, **205** (2024), 748–762.

[7] B.A. Danzomo, S.A. Umar, and M.J.E. Salami, *Wet scrubber design*, M. Mariappan, M.R. Arshad, R. Akmeliawati and C.S. Chong (eds), Control Engineering in Robotics and Industrial Automation, Studies in Systems, Decision and Control, Springer, Cham. **371** (2021).

[8] T. Darbandi, M. Risberg, and L. Westerlund, *Effect of operation conditions on particulate matter removal by a packed-bed wet scrubber for a small-scale biofuel boiler*, Thermal Sc. Eng. Progress, **47** (2024), p. 102290.

[9] T.M. Gantina, P. Iriani, and C.K. Wachjoe, *Biogas purification using water scrubber with variations of water flow rate and biogas pressure*, J. Phys.: Conf. Ser. IOP Pub. **1450** (2020), no. 1, 012011.

[10] P. Goel, A. Moharana, and A.K. Nayak, *Numerical simulation of in-jection characteristics, hydrodynamics and absorption of iodine vapor in a venturi scrubber operating in self-priming mode*, Nuclear Engin. Design **341** (2019), 360–367.

[11] A. Hoyos, A. Joubert, A. Bouhanguel, M. Henry, S. Durécu, and L. Le Coq, *Multiapproach design methodology of a downscaled wet scrubber to study the collection of submicronic particles from waste incineration flue gas*, Processes **12** (2024), no. 8, 1655.

[12] S. Hu, Y. Gao, G. Feng, F. Hu, C. Liu, and J. Li, *Experimental study of the dust-removal performance of a wet scrubber*, Int. J. Coal Sci. Technol. **8** (2021), 228–239.

[13] H. Khadra, R. Kouider, N. Toufik Tayeb, A. Al-Kassir, and J.P. Carrasco-Amador, *Numerical simulation of the cleaning performance of a venturi scrubber*, Energies **15** (2022), no. 4, p. 1531.

[14] B.T.W. Mestemaker, E. Elmazi, L. Van Biert, H.N. Van den Heuvel, and K. Visser, *Modelling and simulation of a wet scrubber system*, Proc. 4th Int. Conf. Modell. Optim. Ship Energy Syst., TU Delft OPEN Publishing, 2024, pp. 155.

[15] S. Mukherjee, A. Verma, S. Biswas, M. Bal, and B.C. Meikap, *Removal of cement dust particulates via fully submerged self-primed Venturi scrubber*, CLEAN–Soil, Air, Water **49** (2021), no. 5, 2000241.

[16] N. Räsänen, P. Mäkelä, M. Lindgren, and O. Pekkala, *Venturi scrubber development and implementation to industry scale*, In Proceedings of the 16th International Ferro-Alloys Congress (INFACON XVI), (2021). https://doi.org/10.2139/ssrn.3926057.

[17] W. Thelin and L. Lin, *CFD-driven investigation on improving heat recovery in centrifugal wet scrubbers*, Int. J. Heat Mass Transfer, **249** (2025), 127251.

[18] A. Tomaszewski, T. Przybylinski, P. Kapica, and M. Lackowski, *Influence of the spray scrubber geometry on the efficiency of dust removal–theoretical predictions and CFD analysis*, J. Appl. Fluid Mech. **13** (2020), no. 4, 1055–1066.

[19] F. Turkoglu and S. Bayraktar, *A numerical study comparing hydro-dynamic performance of circular and square cross-sectional wetted venturi scrubbers*, J. Brazil. Soc. Mech. Sci. Eng. **48** (2026), no. 8.

[20] A. Wansom, P. Maneechot, N. Jiteurtragool, and T. Vitidsant, *PM2.5 collection enhancement in a smart hybrid wet scrubber tower*, Processes **11** (2023), no. 12, 3306.